

Quantitative real-time analysis of nucleolar stress by coherent phase microscopy

Vladimir P. Tychinsky
Alexander V. Kretushev
Ivan V. Klemyashov

Moscow Institute of Radioengineering
Electronics and Automation
78 Vernadsky Avenue
Moscow 119454, Russia

Tatyana V. Vyshenskaya

Moscow State University
Faculty of Physics
4 Leninskie Gory
Moscow 119992, Russia

Natalya A. Filippova
Natan T. Raikhlin
Alexander A. Shtil

Blokhin Cancer Center
24 Kashirskoye shosse
Moscow 115478, Russia

Abstract. We develop a method of coherent phase microscopy (CPM) for direct visualization of nonfixed, nonstained mammalian cells (both cultured cells and freshly isolated tumor biopsies) followed by computer-assisted data analysis. The major purpose of CPM is to evaluate the refractive properties of optically dense intracellular structures such as the nucleus and the nucleoli. In particular, we focus on quantitative real-time analysis of the nucleolar dynamics using phase thickness as an equivalent of optical path difference for optically non-homogenous biological objects. Pharmacological inhibition of gene transcription leads to a dramatic decrease of the phase thickness of the nucleoli within the initial minutes of cell exposure. Furthermore, the acute depletion of intracellular ATP pool, depolymerization of microtubules and inhibition of DNA replication resulted in a rapid decrease of the nucleolar phase thickness. These optical effects were paralleled by segregation of nucleolar components as documented by electron microscopy. Thus, CPM detects early changes of nucleolar dynamics, in particular, the nucleolar segregation as part of general cellular response to cytotoxic stress, regardless of whether the nucleolus is or is not the primary target of the toxin. CPM is applicable for monitoring and quantitative analysis of the “nucleolar stress” in living mammalian cells. © 2008 Society of Photo-Optical Instrumentation Engineers. [DOI: 10.1117/1.3042241]

Keywords: coherent phase microscopy; phase thickness; nucleoli; gene transcription; cytotoxicity.

Paper 08155R received May 12, 2008; revised manuscript received Oct. 1, 2008; accepted for publication Oct. 21, 2008; published online Dec. 30, 2008.

1 Introduction

The interference-based approaches for noninvasive, quantitative analysis of living organisms are aimed at investigating a fundamental link between the refractive properties of biological objects and metabolic processes.^{1–10} The major parameter measured in these methods, i.e., optical path difference (OPD) or path length, has been attributed to distinct morphophysiological states in a variety of objects.^{1,6,8–12} Methods of registering OPD are critical for high spatial and temporal resolution. The multistep method and its modifications^{5,7,13} are based on registration of interference patterns obtained using sequential measurements with fixed values of the reference wave phase, followed by calculation of local values of the object's phase. However, the distribution of intensity in interference patterns is limited by diffraction on aperture, thereby resolution in these images may be insufficient.^{7,13} Another drawback might be the noise due to uncontrollable changes of OPD. Active stabilization significantly decreased noise and enabled achievement⁵ of a prolonged stability of OPD. Use of common-path interferometry made OPD more stable, which, together with Fourier and Hilbert phase microscopy, enabled

registering fast fluctuations of erythrocyte plasma membrane.^{4,6} Hilbert phase microscopy with common path interferometry demonstrated an enhanced precision of measurements, a low sensitivity to vibrations, and a millisecond range of temporal resolution.²

Refractive properties and geometrical thickness may vary across the object, thereby differentially influencing^{1–10} on OPD. To decouple their contributions, the measurements in two immersion media with distinct refractive indices have been proposed.¹ Lue et al. facilitated the decoupling procedure and improved its accuracy by measuring refractive properties of cells placed into microchannels.³ This technique enabled the determination of the geometrical thickness of erythrocytes, and the evaluation of cellular changes during hemolysis.⁶ The values of axial thickness and refractive index in the phase images of neurons and HeLa cells were obtained.^{1,5} Still, these approaches include laborious manipulations that might alter cell viability and refractive properties.

We characterized the OPD measured by the coherent phase microscopy (CPM) of transparent biological objects, as phase thickness.^{8–12} This parameter, detectable by the compensation method, enabled us to describe “optical portraits” of nonfixed, nonstained chloroplasts and spores with high sensitivity and spatial and temporal resolutions.^{10–12} In this study we investi-

Address all correspondence to: Vladimir P. Tychinsky, Moscow Institute of Radioengineering, Electronics and Automation, 78 Vernadsky Avenue, Moscow 119454, Russia. Tel: 495 434-6792; Fax: 495 434-8665; E-mail: vtych@yandex.ru

gate the applicability of CPM for real-time analysis of metabolic changes in high eukaryotes. Nucleoli, the sites of ribosomal biogenesis, are exceptionally sensitive dynamic structures that rapidly respond to a variety of environmental stimuli. The term nucleolar stress encompasses a plethora of structural and functional changes in stimulated cells.^{14,15} Although modern fluorescent-microscopy-based techniques and electron microscopy provide valuable information about the traffic of individual nucleolar proteins in stressed cells,^{16,17} single-cell analysis of nucleolar dynamics in real time requires high spatial and temporal resolution combined with little or no invasiveness into the object. We demonstrate here that CPM can be used for rapid quantitative evaluation of nucleolar stress induced by pharmacological inhibitors of vital cellular processes.

2 Materials and Methods

Human HCT116 colon carcinoma cells (American Type Culture Collection) were propagated in Dulbecco's modified Eagle's medium supplemented with 5% fetal calf serum (HyClone), 2 mM L-glutamine, 100 U/ml penicillin, and 100 $\mu\text{g}/\text{ml}$ streptomycin at 37°C, 5% CO₂. Cells were plated on glass coverslips to reach ~50% confluence by the day of the experiment. Actinomycin D (act D), rotenone in combination with SF6847, oligomycin, aphidicolin, or vincristine were added to the cells followed by CPM. In preliminary experiments, we determined the concentrations of each agent and the time of cell exposure sufficient to block transcription, deplete the intracellular ATP pool, depolymerize the microtubule network, or inhibit DNA replication, respectively.¹⁸⁻²¹ The conditions of cell exposure are presented in Sec. 3 and figure legends. After the completion of exposure the specimens (30 to 100 randomly selected cells per each coverslip) were immediately examined using our original "Airyscan" microscope. For transmission electron microscopy, cells were plated and treated with drugs as already described, then washed once with saline, fixed in 2.5% glutaraldehyde in 0.1 M phosphate buffer, pH 7.3, and stained with 1% OsO₄. After dehydration, the samples were embedded in Epon-812. Ultrathin sections were contrasted with lead salts. Electron microscopy was performed with JEM-1200 EX-11 device (Japan). All reagents were purchased from Sigma-Aldrich unless specified otherwise.

The optical scheme of the Airyscan microscope is shown in Fig. 1(a). The microscope is a modification of a Linnik interferometer with a He-Ne laser ($\lambda=633$ nm) as a source of coherent light. The microscope is equipped with the dissector image tube (Electron, Russia) to register the interference signal, and an electronic unit for computer-assisted cell imaging.⁸ The samples were placed into a cell count chamber fixed on the microscope table. The Olympus lens 20 \times [numerical aperture (NA=0.4)] with a 24- μm view field was used. Measurements of OPD were performed sequentially at each point of the image. To register the interference signal and to convert it into local phase values, a linear periodic modulation of the reference wave phase was performed. The sampling frequency and the image input rate were determined by the modulation frequency of 1 kHz (or 1 ms/pixel). The noise-limited sensitivity was 0.5 nm. Normally the sensitivity of OPD measurements was 2 to 3 nm. The enhanced sensitiv-

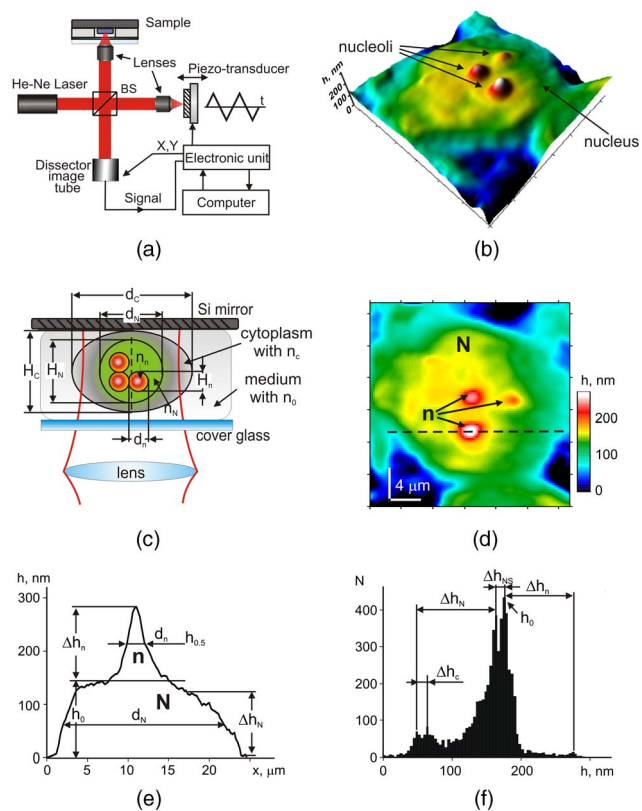


Fig. 1 Physical principle of CPM: (a) optical scheme of the Airyscan microscope, (b) pseudo-3-D phase image of the HCT116 cell, and (c) physical model of the cell in liquid medium. The refractive indices of the cytoplasm n_c , the nucleus n_n , and the nucleolus n_n are volume averaged $n(x, y, z)$. The cross sizes (d_c, d_n, d_n) of the respective structures are assumed equal to the geometric thicknesses (H_c, H_n, H_n). (d) 2-D phase image (topogram) of the same cell with the nucleoli n (arrows) and the section (dotted line); N is the nucleus; and (e) phase height profile $h(x)$ along the section of the image. Shown are the areas that correspond to the nucleus N and the nucleolus n ; d_N and d_n are the diameters of the nucleus and the nucleolus, h_0 is the maximal nuclear phase height, and $h_{0.5}$ is the nucleolar semi-height; and (f) topohistogram showing the dependence of the number of pixels $N(h)$ on the phase thickness h on the topogram $h(x, y)$. The maxima of phase height distribution for the topogram in (d) correspond to the characteristic values Δh_c and Δh_n that are the phase thicknesses of the cytoplasm and the nucleus, respectively; Δh_{NS} is the interval of variations of the phase thickness due to nonhomogeneity of the nucleoplasm in the vicinity of the nucleolus; Δh_n is the phase thickness of the nucleoli.

ity to translational shifts was registered on the steep slopes of the phase height profiles,⁸ thereby facilitating investigation of intracellular processes. The least measured amplitudes (~0.1 nm) of translational oscillations were simulated with piezo actuator.

The software package provided repeatable measurements of OPD profiles recorded as coordinate-time matrices (track charts⁸) along an arbitrarily assigned scan-line, and cell dynamics was presented as spatial-temporal portraits. The software package enabled us to obtain topohistograms and pseudo-3-D images of whole cells and their parts, and to map phase fluctuations.⁸ In this study, we extended our software package by introducing topohistograms that depict the function $N_i(h)$, where N_i is the number of pixels in the topogram

$h(x, y)$ in the interval of phase height values from h_i to $h_i + \Delta h$. Thus, the positions of characteristic points in the topohistograms, such as the maximums, minimums, and squares of individual parts of the topohistograms, can be a quantitative representation of morphological and physiological changes in biological objects.

3 Results and Discussion

The basic principle of CPM is the measurement of local phase height $h(x, y)$ that is linked to refractive indices of the object $n(x, y, z)$ and extracellular medium n_0 by the formula:

$$h(x, y) = \int [n(x, y, z) - n_0] dz. \quad (1)$$

The optically nonhomogenous cell can be represented as a multicomponent structure with different refractive properties. In a pseudo-3-D phase image of the object [Fig. 1(b)] the areas with larger OPDs [see Figs. 1(c) and 1(e)] correspond to optically more dense organelles (namely, the nucleoli). Figure 1(c) shows a model of a cell in liquid medium; the refractive indices of the cytoplasm n_C , the nucleus n_N , and the nucleolus n_n are volume averaged $\langle n(x, y, z) \rangle$. Individual cells were visualized in the optical channel of the microscope, then the topograms of their 2-D phase images [Fig. 1(d)] and phase thickness profiles (sections on 2-D phase images) [Fig. 1(e)] were registered and analyzed. The major dimensions of the nucleus and the nucleolus are shown in the phase thickness profile $h(x)$ [Fig. 1(e)]. Keeping in mind that Fig. 1(c) depicts a simplified model, we determined the characteristic parameters from the profiles of the phase thickness $h(x)$ [Fig. 1(e)] along the lines of image section [(Fig. 1(d), dotted line)]. Here Δh_N and Δh_n are the phase thicknesses of the nucleus and the nucleolus, respectively, and d_N and d_n are the cross sizes of the respective organelle. According to Eq. (1), the phase thickness of the nuclei and the nucleoli is proportional to their axial physical thickness:

$$\Delta h_N = H_N [\langle n(x, y, z)_N \rangle - n_C] = H_N \Delta n_N,$$

$$\Delta h_n = H_n [\langle n(x, y, z)_n \rangle - n_N] = H_n \Delta n_n,$$

where Δn_N and Δn_n are regarded as relative refractivities of the nucleus and the nucleolus, respectively, and H_N and H_n are their physical thicknesses.

The preceding equations reflect only the fact that a cell is an optically nonhomogenous object. Although reliable methods of measuring refractivity of cellular compartments remain to be developed, we attempted to quantitatively assess the nuclear and nucleolar refractivities using approximation models. Figure 1(b) shows that the nucleolar shape was close to spherical ($H_n \cong d_n$). Such an approximation is incorrect when the organelle's shape is elliptic. In this case, we considered the ratio of the axes of the ellipsoid and uncertainty of its orientation to the optical axis. For instance, if axial thickness varies within $H_N \cong (0.5 \text{ to } 2)d_N$ in the nuclear phase profile [(Fig. 1(e))] this results in uncertainty of refractivity within $\Delta n_N = 0.005$ to 0.02 and the nuclear refractive index within

$n_N \cong 1.335$ to 1.35. These considerations were employed for estimation of refractivity in cells exposed to act D (see later in the paper).

To obtain statistically reliable optical parameters of subcellular structures, we used topohistograms [Fig. 1(f)] that illustrate a distribution of the phase thicknesses across the cell. The maxima in the histograms corresponded to the areas in the topogram with close values of the phase thickness, e.g., plain apexes of the nuclear and nucleolar profiles. These areas are the parts of the image with close values of refractive indices and, therefore, with greater statistical impact. Figure 1(f) shows how the phase thicknesses of the cytoplasm Δh_C , the nucleus Δh_N , the nucleoli Δh_n , and the nuclear nonhomogeneities Δh_{NS} were determined. The following parameters were used to analyze the images: the phase height profile $h(x)$, its maximal value Δh (phase thickness), and the horizontal size (or diameter) d of the structural element. In the phase image of the cell [(Fig. 1(d)], the optically dense nucleus and the nucleoli were identified by local increases of the phase thicknesses Δh_N and Δh_n . The contrast of the nucleolus is due to the excess of nucleolar refractive index $\delta n = \Delta n_n - \Delta n_N \cong \Delta h_n / d_n$. Therefore, a higher phase thickness of the nucleolus Δh_n compared to that of the nucleus [Figs. 1(d) and 1(e)] is explained by higher refractive index of the nucleolus.

To analyze nucleolar dynamics by CPM, we exposed mammalian cells to pharmacological agents known to inhibit major cellular functions. In untreated (control) HCT116 cells the nucleolus was visualized as the optically dense zone [(Fig. 2(a)] that became flattened and less dense after the addition of the transcriptional inhibitor act D [(Fig. 2(b)]. The nucleolar phase thickness Δh_n decreased gradually, reaching its lowest value after 30 to 40 min with the drug and then remained low for at least 60 min. Statistically accurate values of Δh_n and Δh_N were determined by characteristic points at the phase height topohistograms. The topohistograms in Figs. 2(c) and 2(d) [drawn for phase images in Figs. 2(a) and 2(b)] demonstrated the changes in distribution of the phase heights within the nucleus Δh_N and the nucleolus Δh_n . The statistically minimal phase thickness of the nucleus corresponded to $\Delta h_N = 155$ nm [(Fig. 2(c)]. The maximum at $h_0 = 205$ nm was attributed to the maximal value of the nuclear phase thickness [see Figs. 1(e), 2(e), and 2(f)]. The values above this maximum were interpreted as the phase thickness of the nucleolus $\Delta h_n = 84$ nm. The nucleolar phase thickness Δh_n in act D-treated cells decreased markedly ($\Delta h_n = 22$ nm) [compare Figs. 2(c) and 2(d)]. These data indicate that act D decreased the nucleolar phase thickness Δh_n approximately threefold. Furthermore, a decreased phase thickness of the nucleoli was observed in other human carcinoma (HeLa and MCF-7) or murine fibroblast (NIH 3T3) cell lines exposed to act D. This optical effect was also detectable in tumor specimens isolated from patients' biopsies (not shown). These results indicate that the decreased phase thickness of the nucleoli is a hallmark of transcriptional blockade in various mammalian cell types. The optical characteristics of the nucleoli changed during the initial minutes of cell exposure to act D. To characterize these changes we used the isolines at the level of the phase semithickness $h_{0.5}$ of the nucleolus [see Figs. 2(e) and 2(f)]. The nucleolar phase thickness was determined as the excess

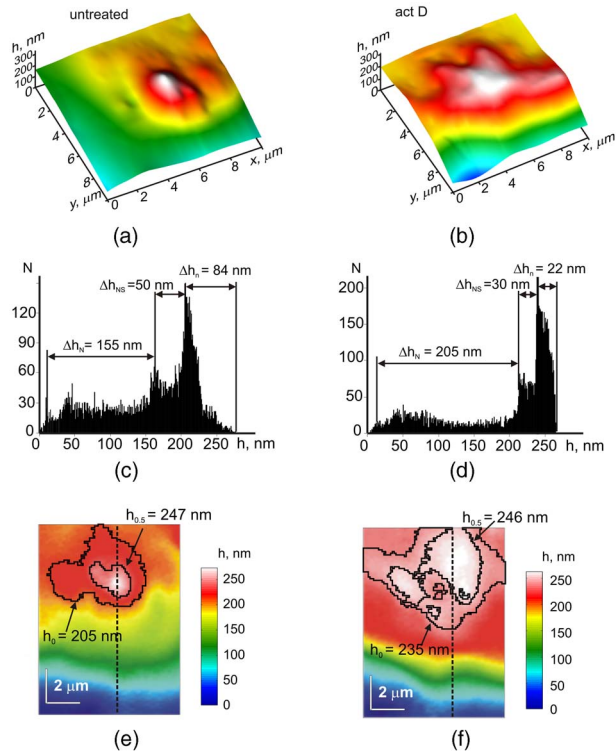


Fig. 2 CPM-based single-cell analysis: (a), (c), and (e), untreated HCT116 cell; (b), (d), and (f), the same cell treated with $0.1 \mu\text{M}$ act D for 30 min. (a) and (b) are phase images of the nucleolus and an adjacent region. Due to higher optical density, the nucleolus is detectable over the background of the nucleus. (c) and (d) are the values of phase thicknesses of the nucleoli Δh_n and the nuclei Δh_N determined from characteristic points in the histograms of phase thicknesses for the entire area of the phase image in (a) and (b). The differences between h_0 and Δh_N were interpreted as Δh_{NS} . (e) and (f) are 2-D phase images [corresponding to (a) and (b)] before and after the addition of act D. The outer contours connect the levels of the phase height h_0 and reflect the minute nonhomogeneities of the nucleoplasm around the nucleolus. The inner contours connect the levels of the phase height at the nucleolar semiheight $h_{0.5}$, reflecting the geometric projection of the nucleolus on the image plane. In act D treated cells the decreased nucleolar phase thickness was associated with an increase of the area of the nucleolus within the line $h_{0.5}$ (f).

above the main maximum h_0 in the histograms of the nuclear phase thickness [Figs. 1(e), 2(c), and 2(d)]. In the majority of untreated cells, the shape of the nucleoli was close to elliptic [Fig. 3(a)]. The minimal diameter at the nucleolar semiheight was $\cong 1.6 \mu\text{m}$, whereas the maximal diameter was $\cong 2.4 \mu\text{m}$. The initial phase thickness values were $\Delta h_n = 80$ to 100 nm , and the nucleolar shape changed slowly (within several minutes). The amplitude of these slow changes was $< 20 \text{ nm}$. According to these results, the nucleolar refractivity (calculated with the approximations already discussed) of untreated cells was relatively high: $\delta n \cong 0.04$ to 0.06 . In act D-treated cells the shape of the nucleoli changed rapidly. By 6 min with the drug, the nucleolar shape switched from elliptic to spherical and again to elliptic, and the diameter varied within 4.0 to $5.5 \mu\text{m}$. The phase thickness was $\Delta h_n = 50 \text{ nm}$ [Fig. 3(b)]. During next 6 min, the nucleolar diameter became smaller (from 5 to $2 \mu\text{m}$), while the spherical shape remained unchanged. The phase thickness Δh_n was approximately

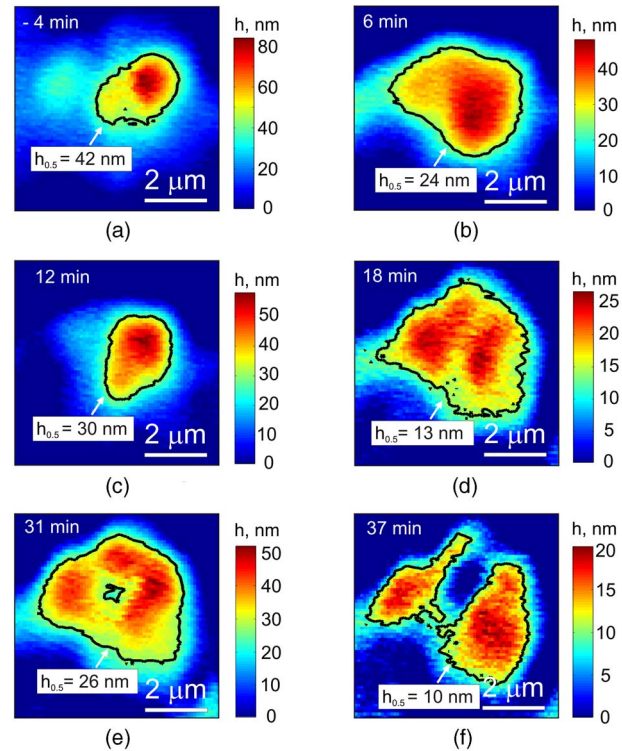


Fig. 3 Time course of phase thickness changes in act D-treated HCT116 cell. Images of the individual cell were captured at indicated time intervals 4 min before (a) and within 37 min after the addition of act D (b) to (f). Images show the isolines of the nucleolar phase semiheights ($h_{0.5}$). The values $h_0 = 0$ were obtained from the respective histograms. The phase heights of individual structural elements relative to background were evaluated using the colored scale. (Color online only.)

60 nm [Fig. 3(c)], which could be associated with a decreased refractivity $\delta n \cong 0.01$ to 0.015 . By 18 min, we registered two elliptic components with equal phase thickness ($\Delta h_n = 24 \text{ nm}$). Each component was 1.5 to $2 \mu\text{m}$ in diameter [Fig. 3(d)]. By 31 min with the drug, the components of the nucleolar phase image became even more contrasted, and the nucleolus acquired the shape of the ring, with the phase thickness $\Delta h_n = 52 \text{ nm}$ [Fig. 3(e)]. During another 6 min, the phase thickness decreased, the ring-shaped image disappeared, and the phase thickness reduced to 20 nm [Fig. 3(f)]. By 37 min, the nucleolus was visualized as two near-oval components. By this time, the nucleolus was undetectable over the nuclear background. These data indicate that distribution of optically dense and sparse zones was uneven. Thus, the response of the nucleoli to the transcriptional inhibitor was more complex than a uniform drop of the phase thickness. The nucleoli not merely became less dense; rather, the phase thickness was relocated across the nucleolus. Nevertheless, the major trend of the effect of act D was the decreased nucleolar phase thickness.

Next, we determined which changes of nucleolar ultrastructure underlie the optical parameters detectable by CPM. In untreated HCT116 cells, the shape of the nucleoli was elliptic. The homogenous, low-electron-density material (fibrillar centers) was surrounded by electron dense zones (dense fibrillar component). The granular component was detectable

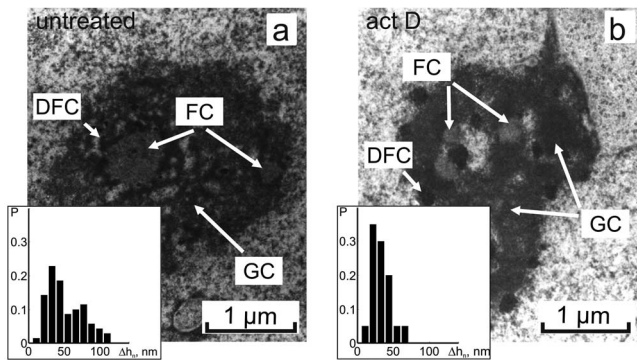


Fig. 4 Nucleolar segregation is associated with decreased nucleolar phase thickness in act D-treated cells. HCT116 cells were (a) left untreated or (b) treated with $0.1 \mu\text{M}$ act D for 15 min followed by CPM. A portion of cells from the same specimen was processed for transmissive electron microscopy. Here and in Fig. 5: GC, granular component; FC, fibrillar center; DFC; dense fibrillar component (shorter arrows). Morphological signs of nucleolar segregation in response to act D are discussed in the text. In histograms (insets): the x axis is the phase thicknesses of the groups of nucleoli and the y axis is the statistical probabilities of each group.

at the periphery and in the center of the nucleoli [Fig. 4(a)]. In striking contrast, exposure to act D rapidly caused an enlargement of fibrillar centers and dense fibrillar components and a decrease of electron density of the granular component and fibrillar centers [Fig. 4(b)]. Dense fibrillar material was redistributed. These phenomena indicated the nucleolar segregation, a hallmark of morphological and functional events that comprise the reaction of the nucleoli to transcriptional inhibition²² by act D. Nucleolar segregation was associated with a substantial decrease of the nucleolar phase thickness in act D-treated cells [Figs. 4(a) and 4(b), insets]. We then investigated the changes of nucleolar phase thickness and ultrastructure evoked by various toxic stimuli. As shown in Fig. 5(b), energy depletion with rotenone plus SF6847 caused a decrease of electron density of fibrillar centers and the granular component. The fibrillar centers and the dense fibrillar component were shifted to the periphery of the nuclei. Likewise, oligomycin caused drastic changes of the shape of the nucleoli; the nucleolar electron density and the size of fibrillar centers decreased markedly in a way similar to that in Fig. 5(b). Exposure to the replication blocker aphidicolin dropped the nucleolar electron density; the granular component prevailed, whereas fibrillar centers and fibrillar component were much less detectable [Fig. 5(c)]. Interestingly, in aphidicolin-treated cells a portion of the nucleoli retained relatively high phase thickness [$\Delta h_n \cong 60$ to 90 nm; Fig. 5(c)]. We tend to explain this finding by the facts that the cells in S phase are vulnerable to aphidicolin,²⁰ and DNA replication is mechanically coupled to transcriptional machinery.²³ Thus, aphidicolin might hamper transcription in replicating cells. Because we worked with nonsynchronized cell culture, only a part of cells should be in S phase at the time of CPM analysis; it is probably these cells that responded to aphidicolin by decreased Δh_n . Fragmentation of the nucleoli and a decreased electron density of these organelles were observed upon treatment with vincristine [Fig. 5(d)]. Therefore, each metabolic poison caused rapid (within the initial 15 to 30 min of cell

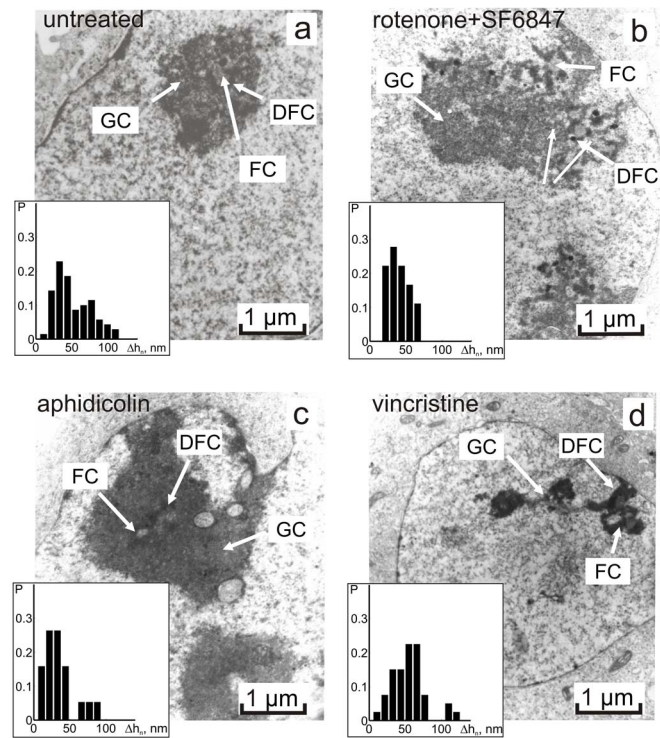


Fig. 5 Nucleolar segregation and a decrease of nucleolar phase thicknesses in response to various agents. HCT116 cells were (a) left untreated or treated as follows: (b) $50 \mu\text{M}$ rotenone + $1 \mu\text{M}$ SF6847, 15 min; (c) $10 \mu\text{M}$ aphidicolin, 30 min; and (d) $0.1 \mu\text{M}$ vincristine, 30 min. The electron microscope images and histograms are labeled as in Fig. 4. See text for details of nucleolar segregation.

exposure) decrease of the nucleolar phase thickness that was paralleled by irregularity of the nucleolar shape; decreased density of fibrillar and granular components; and fragmentation of the nucleoli, the morphological signs of nucleolar segregation.^{24–26}

Thus, the decreased phase thickness of the nucleoli is an optical signature of the nucleolar segregation in stressed cells. Moreover, rapid decrease of the phase thickness is a typical event associated with the response to toxins in chloroplasts, spores and isolated mitochondria.¹⁰ Therefore, the decreased phase thickness should be considered a fundamental phenomenon common for different objects exposed to a variety of stress stimuli. This, in turn, presumes the commonality of the mechanism(s) that underlie this effect. One can hypothesize that the optical density in biological objects is largely related to the physical state of proteins and water. Chromatin condensation and protein misfolding, the phenomena characteristic for transcriptional inhibition, might be associated with a decrease of hydrated shells that supposedly contain water molecules with enhanced electron susceptibility.^{8,27,28} Therefore, transcriptional block (and perhaps other metabolic inhibitors) would cause a decrease of effective electric charges on proteins (due to more dense packaging of proteins), the accumulation of misfolded macromolecules, and a smaller share of bound water molecules. These events would be manifested in a decreased volume-averaged refractive index determined by CPM.

4 Conclusion

The CPM-based analysis required no fixation or staining of cells, and enabled rapid detection of nucleolar morphology and physiology affected by various toxins. The quantitative data generated by CPM, i.e., the phase thickness, lateral dimensions, and refractive index, are associated with nucleolar segregation in stressed cells. The optical effects in the nucleoli are similar to those found in isolated organelles and prokaryotes exposed to metabolic poisons, strongly suggesting that the CPM parameters reflect the responses common for different biological objects. The topohistograms of phase height distribution generated in CPM may be applicable for rapid, quantitative, and inexpensive screening of novel cytotoxic (e.g., anticancer) drugs using the nucleolar stress as a readout.

Acknowledgments

This work was supported by grants from the Russian Foundation for Basic Research (07-04-00473, 08-04-12104-ofi), grants from the President of Russian Federation (Young Scientists Support Program; MK-4614.2006.4), and from the Protec company.

References

- B. Rappaz, P. Marquet, E. Cuche, Y. Emery, C. Depeursinge, and P. Magistretti, "Measurement of the integral refractive index and dynamic cell morphometry of living cell with digital holographic microscopy," *Opt. Express* **13**(23), 9361–9373 (2005).
- G. Popescu, K. Badizadegan, R. R. Dasari, and M. Feld, "Observation of dynamic subdomains in red blood cells," *J. Biomed. Opt.* **11**(4), 040503-1–040503-3 (2006).
- N. Lue, G. Popescu, T. Ikeda, R. Dasari, K. Badizadegan, and M. Feld, "Live cell refractometry using microfluidic devices," *Opt. Lett.* **31**(18), 2759–2761 (2006).
- T. Ikeda, G. Popescu, and R. R. Dasari, "Hilbert phase microscopy for investigating fast dynamics in transparent systems," *Opt. Lett.* **30**(10), 1165–1168 (2005).
- H. Iwai, C. Fang-yen, G. Popescu, A. Wax, K. Badizadegan, R. Dasari, and M. Feld, "Quantitative phase imaging using actively stabilized phase-shifting low-coherence interferometry," *Opt. Lett.* **29**(20), 2399–2401 (2004).
- G. Popescu, T. Ikeda, C. Best, K. Badizadegan, R. Dasari, and M. Feld, "Erythrocyte structure and dynamics quantified by Hilbert phase microscopy," *J. Biomed. Opt.* **10**(6), 060503-1–060503-3 (2005).
- N. Lue, W. Choi, G. Popescu, T. Ikeda, R. Dasari, K. Badizadegan, and M. Feld, "Quantitative phase imaging of live cells using fast Fourier phase microscopy," *Appl. Opt.* **46**(10), 1836–1842 (2007).
- V. P. Tychinsky, "Coherent phase microscopy: is the 'dialog' with a cell possible?" *Phys. Usp.* **50**(5), 535–552 (2007).
- V. Tychinsky, A. Kretushev, and T. Vyshenskaja, "Mitochondria optical parameters are dependent on their energy state: a new electrooptical effect?" *Eur. Biophys. J.* **33**(8), 700–705 (2004).
- V. P. Tychinsky, A. V. Kretushev, T. V. Vyshenskaya, and A. N. Tikhonov, "Coherent phase microscopy in cell biology: visualization of metabolic states," *Biochim. Biophys. Acta* **1708**(3), 362–366 (2005).
- V. P. Tychinsky, A. V. Kretushev, T. V. Vyshenskaya, and A. N. Tikhonov, "A dynamic phase microscopy study of optical characteristics of individual chloroplasts," *Biochim. Biophys. Acta* **1665**(1–2), 57–64 (2004).
- V. P. Tychinsky, Y. A. Nikolaev, V. V. Lisovskii, A. V. Kretushev, T. V. Vyshenskaja, A. L. Mulukin, N. E. Suzina, V. I. Duda, and G. I. El'-Registan, "Dynamic phase microscopy, a new method to detect viable and killed spores and to estimate the heterogeneity of spore populations," *Adv. Space Res.* **40**, 1678–1685 (2007).
- J. Millerd, N. Brock, J. Hayes, M. North-Morris, M. Novak, and J. Wyant, "Pixelated phase-mask dynamic interferometer," *Proc. SPIE* **5531**, 304–316 (2005).
- M. Olson, "Sensing cellular stress: another new function for the nucleolus?" *Sci. STKE* **224**, 10 (2004).
- C. Mayer, H. Bierhoff, and I. Grummt, "The nucleolus as a stress sensor," *Genes Dev.* **19**(8), 933–941 (2005).
- M. Derenzini, G. Pasquinelli, M.-F. O'Donohue, D. Ploton, and M. Thirty, "Structural and functional organization of ribosomal genes within mammalian cell nucleolus," *J. Histochem. Cytochem.* **54**(2), 131–145 (2006).
- S. Jakobs, "High resolution imaging of live mitochondria," *Biochim. Biophys. Acta* **1763**(5–6), 561–575 (2006).
- K. Kalita, D. Makonchuk, C. Gomes, J.-J. Zheng, and M. Hetman, "Inhibition of nucleolar transcription as a trigger for neuronal apoptosis," *J. Neurochem.* **105**(6), 2286–2299 (2008).
- M. Shamoto-Nagai, W. Maruyama, Y. Kato, K. Isobe, M. Tanaka, M. Naoi, and T. Osawa, "An inhibitor of mitochondrial complex I, rotenone, inactivates proteasome by oxidative modification and induces aggregation of oxidized proteins in SH-SY5Y cells," *J. Neurosci. Res.* **74**(4), 589–597 (2003).
- D. Schechter, V. Costanzo, and J. Gautier, "Regulation of DNA replication by ATR: signaling in response to DNA intermediates," *DNA Repair* **3**(8–9), 901–908 (2004).
- M. N. Islam and M. N. Iskander, "Microtubulin binding sites as target for developing anticancer agents," *Mini-Rev. Med. Chem.* **4**(10), 1077–1104 (2004).
- Y. Shav-Tal, J. Blechman, X. Darzacq, C. Montagna, B. T. Dye, J. G. Patton, R. H. Singer, and D. Zipori, "Dynamic sorting of nuclear components into distinct nucleolar caps during transcriptional inhibition," *Mol. Biol. Cell* **16**, 2395–2413 (2005).
- E. V. Mirkin, D. Castro Roa, E. Nudler, and S. M. Mirkin, "Transcription regulatory elements are punctuation marks for DNA replication," *Proc. Natl. Acad. Sci. U.S.A.* **103**(19), 7276–7281 (2006).
- M. Thiry, J. M. Jamison, J. Gilloteaux, J. L. Summers, and G. Goessens, "Ultrastructural nucleolar alterations induced by an ametrantone/poly(r(A-U)) complex," *Exp. Cell Res.* **236**(1), 275–284 (1997).
- J. M. Jamison, J. Gilloteaux, M. Thiry, M. Authélet, G. Goessens, and J. L. Summers, "Ultrastructural nucleolar alterations induced by an ametrantone--poly r(A-U) complex," *Tissue Cell* **30**(4), 475–484 (1998).
- D. Krajčí, V. Mares, V. Lisá, A. Spanová, and J. Vorlíček, "Ultrastructure of nuclei of cisplatin-treated C6 glioma cells undergoing apoptosis," *Eur. J. Cell Biol.* **79**(5), 365–376 (2000).
- Y. Yamasaki, Y. Teramoto, and K. Yoshikawa, "Disappearance of the negative charge in giant DNA with folding transition," *Biophys. J.* **80**(6), 2823–2832 (2001).
- Y. Levy and J. N. Onuchic, "Water mediation in protein folding and molecular recognition," *Annu. Rev. Biophys. Biomol. Struct.* **35**, 389–415 (2006).